Title

The strength of the Earth’s magnetic field from Pre-Pottery to Pottery Neolithic, Jordan

Journal

Proceedings of the National Academy of Sciences of the United States of America, 118(34)

ISSN

0027-8424

Authors

Di Chiara, Anita
Tauxe, Lisa
Levy, Thomas E
et al.

Publication Date

2021-08-24

DOI

10.1073/pnas.2100995118

Peer reviewed

The strength of the Earth's magnetic field from Pre-Pottery to Pottery Neolithic, Jordan

Anita Di Chiara[a,b], Lisa Tauxe[b,1], Thomas E. Levy[c], Mohammad Najjar[d], Fabio Florindo[a], and Erez Ben-Yosef[e]

[a]Istituto Nazionale di Geofisica e Vulcanologia, 00143 Roma, Italy; [b]Scripps Institution of Oceanography, University of California San Diego, La Jolla, CA 92093-0220; [c]Levantine Archaeology and Cyber-Archaeology Laboratory, University of California San Diego, La Jolla, CA 92093; [d]Council for British Research in the Levant (CBRL), Tla' Al-Ali, Amman 11181, Jordan; and [e]Department of Archaeology and Ancient Near Eastern Cultures, Tel Aviv University, Tel Aviv 6997801, Israel

Contributed by Lisa Tauxe, June 28, 2021 (sent for review January 17, 2021; reviewed by Maxwell Brown and Monika Korte)

Constraining secular variation of the Earth's magnetic field strength in the past is fundamental to understanding short-term processes of the geodynamo. Such records also constitute a powerful and independent dating tool for archaeological sites and geological formations. In this study, we present 11 robust archaeointensity results from Pre-Pottery to Pottery Neolithic Jordan that are based on both clay and flint (chert) artifacts. Two of these results constitute the oldest archaeointensity data for the entire Levant, ancient Egypt, Turkey, and Mesopotamia, extending the archaeomagnetic reference curve for the Holocene. Virtual Axial Dipole Moments (VADMs) show that the Earth's magnetic field in the Southern Levant was weak (about two-thirds the present field) at around 7600 BCE, recovering its strength to greater than the present field around 7000 BCE, and gradually weakening again around 5200 BCE. In addition, successful results obtained from burnt flint demonstrate the potential of this very common, and yet rarely used, material in archaeomagnetic research, in particular for prehistoric periods from the first use of fire to the invention of pottery.

archaeointensity | Jordan | Pre-Pottery Neolithic | Neolithic

Archaeomagnetism, the investigation of magnetic properties of archaeological materials, can provide invaluable information on both archaeological chronologies and the geomagnetic field variations in the past. Archaeological materials, fired during their making and/or use, acquire a thermal remanent magnetization (TRM). Such TRMs can constitute a reliable and high-resolution recorder of variations in the Earth's magnetic field (EMF) (1, 2). Fortunately, the process of firing ceramics and flints typically involved sufficiently high temperatures to record a TRM (e.g., ref. 3). While cooling from high temperature, they can preserve a record of the strength (paleointensity) of the EMF and its variation over time. While pottery (along with several other clay-based materials, such as kilns and hearths) are considered reliable archaeomagnetic materials and are widely investigated in archaeomagnetic studies, the use of flint (4) is far less common (5–8). Indeed, despite being the most common raw material for stone-artifact manufacturing in the Paleolithic (4), it usually bears a weak magnetization, being composed of diamagnetic micro- to crypto-crystalline quartz. Flint's magnetization is derived from detrital impurities and, therefore, is highly variable, reflecting varying degrees of enhancement of magnetic properties upon heating, a result of magnetite formation (e.g., refs. 5 and 9), and its use for archaeomagnetic studies has just begun to be explored (6–8). It should be noted that the potential contribution of heated flint to archaeomagnetic research is substantial. Deliberate heating of flint was part of tool-production processes, as it improves the results of knapping [striking flint in order to produce flakes, sharper cutting edges, and shape tools (10)]. This was widely practiced at least as early as the Upper Paleolithic [~50,000 y (50 ky) B.P. (11)].

In addition to often having a nearly ideal and stable magnetic mineralogy (characterized by stable single domain magnetite or hematite; e.g., ref. 12), the ages of archaeological materials can often be well constrained by using archaeological and historical contexts, as well as radiocarbon dating. Therefore, archaeological materials can be ideal for studying the decadal to centennial (secular) variations of the EMF over time and different regions. Indeed, while more than 90% of the geomagnetic field can be described approximately as a dipole requiring only one measurement over the globe to constrain its value, the rest of the field (the nondipolar components) need to be constrained with synchronous measurements over the entire globe.

Over the last 10 ky, one of the most remarkable features in the history of the Holocene geomagnetic field record is the extremely high strength and rapid variation first recognized in archaeomagnetic data from Syria (13) and confirmed and amplified in several other studies from Israel and Jordan (14–18). Cai et al. (19) defined a "spike" for features with virtual axial dipole moments (VADMs) in excess of ~160 ZAm^2 (where Z is Zetta = 10^{21}). According to this definition, spikes occurred at least twice, first during the 10th century (c.) BCE and then during the 8^{th} c. BCE, a feature now called the Levantine Iron Age Anomaly, or LIAA (18, 20). The rapidity and magnitude of the Levantine spike was at first quite controversial (e.g., ref. 21), but has since been recognized in Mesopotamia (22), Georgia (20), Turkey (23), and several other locations. Yet, the LIAA poses new questions on how fast the magnetic field can change and the spatial extent of such features.

The regional extent of the Levantine spike was addressed in part by Cai et al. (24), who suggested that it may have had a

Significance

The Earth's magnetic field has changed significantly in the past with implications for related phenomena, such as deep-Earth processes and evolution of life. Accurate datasets of its past behavior also provide a dating tool. We present data from Neolithic ceramics and flint from Jordan. Our results are among the oldest in the Levant, covering a period of major changes in human history. The data help in refining the resolution of the archaeomagnetic curve, in turn enhancing its use as a dating tool and for understanding past field behavior. Moreover, we demonstrate the potential for the use of flint material, the most common raw material for the manufacturing of tools in the entire Paleolithic and younger periods, for archaeointensity investigations.

Author contributions: L.T. and E.B.-Y. designed research; A.D.C., T.E.L., and M.N. performed research; A.D.C. and L.T. contributed new reagents/analytic tools; A.D.C., L.T., and E.B.-Y. analyzed data; A.D.C., L.T., T.E.L., and E.B.-Y. wrote the paper with contributions from F.F.; M.N. provided archaeological context; and F.F. provided support for the first author.

Reviewers: M.B., University of Minnesota; and M.K., Helmholtz Centre Potsdam-GFZ German Research Centre for Geosciences.

The authors declare no competing interest.

[1]To whom correspondence may be addressed. Email: ltauxe@ucsd.edu.

Published August 16, 2021.

precursor in China, which subsequently migrated westward, or, given the uncertainty in the age of the Chinese spike, could also have varied nearly synchronously with the Levant. The analysis of Korte and Constable (25) explained the Levantine anomaly as resulting from a normal flux patch at the core–mantle boundary that grew and decayed in situ. Their estimate for the rate of change of the LIAA is about 61 ZAm^2 per c. A contrasting view was presented by Osete et al. (26), who explained the LIAA as resulting from a normal flux patch below the Arabian Peninsula spiking at around 950 BCE. In their model, the flux patch expanded toward the northwest as it decreased in intensity, reaching Iberia at around 750 BCE. Later, at around 600 to 500 BCE, it (or another flux patch) grew below the European continent prior to vanishing.

Such rapid, short-lived, and apparently small-scale variations may have happened multiple times in the past, but older data have a much lower resolution (centennial or even millennial scale), and such variations remain undetected. Archaeomagnetic materials give the unique opportunity to study such variations and improve our understanding of the Holocene variations in the geomagnetic field. For instance, a recent study on New Zealand hearths showed evidence of newly detected high field values with short-lived intensities during the 15^{th} c. CE (27).

Importantly, rapid variations in the EMF can be the basis for using archaeomagnetism as a high-resolution, independent, and robust dating tool in archaeology (e.g., refs. 28, 29), especially when the radiocarbon calibration curve is flat, resulting in very large uncertainties in radiocarbon-derived ages. In such times, it is possible to use paleosecular variation (PSV) records to provide ages (28, 30, 31). Archaeomagnetic dating is based on the statistical comparison of the archaeomagnetic data with the expected values from a reference regional curve (32, 33).

Fig. 1 shows the current paleointensity dataset available on GEOMAGIA50 (34) for Mesopotamia and the Middle East from between 25 and 37°N and 28 and 43°E (within an ∼700-km radius from the localities investigated in this study). From the available dataset of 679 entries, we excluded studies for which the paleointensity data cannot be deemed reliable: results obtained with no alteration check during laboratory experiments, with no dating methods specified, and data with paleointensity site-level dispersion, σ, greater than 15 ZAm^2. A total of 21% of entries were thus excluded and are shown as gray crosses in Fig. 1. We find, therefore, that the ultimate

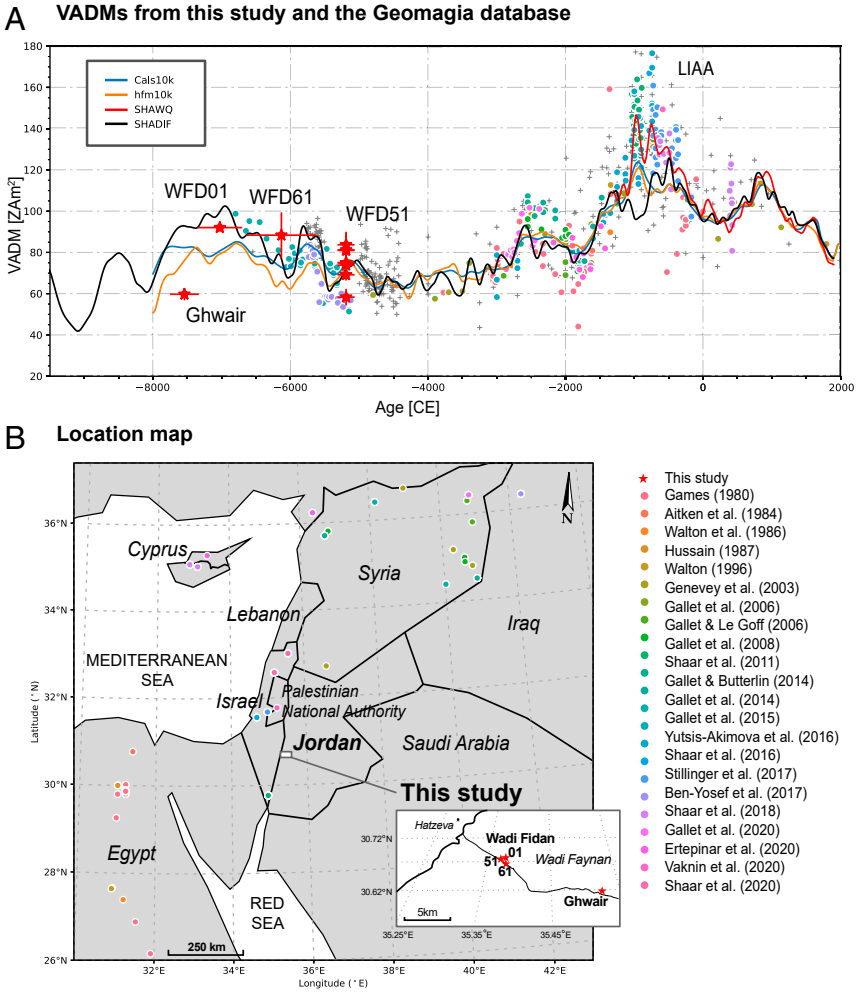

Fig. 1. (*A*) Comparison between the results from the paleointensity analyses from this study (archaeointensity samples represented as red stars) and the data from previous studies available in the GEOMAGIA50 (ref. 34; gray crosses for the data that are not deemed robust), expressed as VADM in ZAm^2 (=10^{21} Am^2). The blue and orange curves are the two synthetic PSV curves from Cals10k.2 and hfm10k global models (35), respectively, and the black and red curves represent the two PSV curves from SHA.DIF.14K (36) and SHAWQ2k (26, 37), respectively, calculated at the coordinates of the study area. (*B*) Location of archaeointensity data from literature used in *A*. (*Inset*) Location of the four archaeological excavations of this study (the Wadi Faynan region, Jordan).

limit on the use of archaeomagnetism as a dating tool is that the archaeomagnetic dataset, despite recent advances, remains sparse for ages older than 3000 BCE for the region under investigation.

Given spherical harmonic models for geomagnetic field variations (e.g., refs. 35–37), the geomagnetic field vector can be estimated at any location on the surface of the Earth. Due to the paucity of archaeomagnetic data from 8000 to 6000 BCE, these models need to rely on sedimentary data, typically smoothed and with an age model less accurate than the one obtained from archaeomagnetic studies (blue and orange curves in Fig. 1). The SHA.DIF.14K model of Pavón-Carrasco et al. (36) (black line in Fig. 1) covers the last 14 ky, and it is based solely on archaeological and volcanic records for the last 9 ky. The most recent models, SHAWQ2k and SHAWQIA of Campuzano et al. (37) and Osete et al. (26), respectively, are the most accurate for the Levantine region, as they are based on a selection of data that passed some rigorous quality criteria. However, combined, they only cover the last 3 ky (red line in Fig. 1). Overall, it is seems that the field's strength was at its lowest value of 40 ZAm^2 at $\sim$9000 and 60 ZAm^2 at $\sim$8000 BCE, it rapidly increased up to 100 ZAm^2 at $\sim$7000 BCE, and then gradually decreased. Since $\sim$6000 BCE, it varied around a constant value of about 70 ZAm^2 until 2000 BCE. From $\sim$1700 to $\sim$900 BCE, the field increased rapidly up to values of 180 ZAm^2, the highest value of the Holocene (Fig. 1*A*).

The Neolithic period witnessed some of the most important cultural revolutions in recent human prehistory, especially the transition from foraging to farming and sedentary societies (38, 39). Because of the archaeological importance of this time period, expanding and refining the independent dating tool of archaeomagnetism would be a major step forward in the study of the Neolithic period. Regrettably, the temporal resolution of the data during the Levantine Neolithic period dramatically decreases with increasing age until only one study is available from Raqqa and Tell Halula, in Syria (40), and no data are available at all for ages older than 6800 BCE. Because of the apparent reduced variability of the magnetic field strength and the scarcity of data, improving its resolution is a primary aim of archaeomagnetism for the Neolithic. Here, we present archaeointensity results from Jordan using ceramic fragments and flint blades; these are radiocarbon-dated at between 7752 and 5069 BCE, thus from the Pre-Pottery Neolithic (B and C) to the Pottery Neolithic period, a time nearly devoid of data so far.

The Levantine archaeological sites selected for this study span the Middle Pre-Pottery Neolithic B (PPNB; circa [ca.] calibrated ^{14}C years B.P. 10100 to 9250), Late PPNB (calibrated ^{14}C years B.P. 9250 to 8250), and Pottery Neolithic (calibrated ^{14}C years B.P 8250 to 6600) (38, 41–43), constrained with radiocarbon dating on charcoal wood remains based on long-lived samples. This sequence is important for understanding a number of issues in global archaeology, including the origins of the village as a settlement type (44), the domestication of plants and animals, and the rise of the Mediterranean diet.

Results

We analyzed six to eight pieces ("specimens") per archaeological fragment ("sample"), three fragments—two pottery sherds and a burnt clay torso—from Ghwair, five flint fragments from Wadi Fidan 01, two ceramic fragments from Wadi Fidan 61, and nine ceramic fragments from Wadi Fidan 51 (Tables 1 and 2 and *Archaeological Context*; see Fig. 5). From a total of 129 specimens, we measured and mass-normalized the Natural Remanent Magnetization (NRM) and susceptibility (χ) for what is here called the Firing Efficiency (FE) ratio (Fig. 2 and *FE Ratio Analyses*) and carried out the IZZI method (see *Methods* and refs. 45, 46) for absolute paleointensity (Table 1, Fig. 3, and *Paleointensity Analyses*).

FE Ratio. The ratio between susceptibility (χ) and the NRM data (both mass normalized with remanence in units of $10^{-3}\mathrm{Am}^2$/kg

Table 1. Archaeointensity results from Pre-Pottery Neolithic and Pottery Neolithic of Jordan

Collection	Cal. age (2σ BCE)	Lat.	Lon.	Sample	Material	Context	*n*/*N*	Uncorr. int	Corr. int	VADM
Ghwair	7752 to 7337	30.6233	35.5061	GHU01574	Ceramic	3.8	0/7	...	...	...
				GHU01272	Burnt clay	12.5	0/7	...	...	...
				GHU01571	Ceramic	3.8	6/7	27.7± 3.8	30.7±1.6	59.5±3.1
WFD01	7450 to 6697	30.6749	35.3718	WF10074	Flint	16	0/5	...	...	...
				WF10095	Flint	16	2/6	...	...	...
				WF102661	Flint	37	2/6	...	...	...
				WF102662	Flint	37	1/6	...	...	...
				WFB10266	Flint	37	3/6	54.0 ± 1.6	47.5± 0.4	92.0 ± 0.7
WFD61	6646 to 5623	30.6686	35.3793	WF134142	Ceramic	2	0/10	...	...	...
				WF132580	Ceramic	2	4/6	48.8± 5.2	45.6± 5.7	88.4±11.1
WFD51	5316 to 5069	30.6724	35.3801	WF12575A	Ceramic	601	3/6	36.4 ±3.0	30.1±2.1	58.3±4.1
				WF12575B	Ceramic	601	6/6	54.7± 5.7	43.2± 3.3	83.7± 6.3
				WF12575D	Ceramic	601	5/6	42.0± 4.7	35.7± 1.4	69.2±2.8
				WF12575E	Ceramic	601	6/6	37.0± 2.1	38.5± 0.9	74.6± 1.7
				WF12575G	Ceramic	601	0/8	...	...	...
				WF12575H	Ceramic	601	8/8	46.9± 3.3	41.9± 1.4	81.2 ± 2.7
				WF12575I	Ceramic	601	7/8	43.7± 4.0	41.8± 4.4	81.0 ±8.5
				WF12575L	Ceramic	601	6/6	45.2± 3.9	38.7± 1.9	75.0±3.7
				WF12575M	Ceramic	601	7/8	46.8± 3.3	38.1± 3.2	73.6± 6.2
							7/9		*38.5±4.2*	*74.6±8.1*

Sample here refers to the paleointensity sample name (individual archaeological fragment), and it corresponds also to a paleointensity site, where the age and magnetic properties are expected to be uniform. Cal. ages (BCE) are radiocarbon ages recalibrated as in Table 2. Lat. and Lon. are the latitude (°N) and longitude (°E), respectively. The archaeological context is reported as locus number. The intensity (int.) results before (uncorr.; uncorrected) and after (corr.; corrected) the correction for cooling rate and anisotropy of the thermal remanence are reported both in μT (and 1σ) and as VADMs in ZAm^2 ($\mathrm{Z} = 1\mathrm{e}^{-21}$). *n*/*N*, number of specimens that gave reliable paleointensity results vs. the total number of specimens analyzed. In italics, the average intensity value is calculated for the collection WFD51.

Table 2. Radiocarbon dates

Site and lab code	Context	Uncal. date, y B.P.	Date Cal BCE (IntCal20, 2σ)
Ghwair I (60)			
Hd17220-17550	Str III	8,627 ± 46	7748 to 7579
Beta140758	Str III	8,620 ± 50	7752 to 7543
Beta140759	Str III	8,610 ± 50	7744 to 7541
Beta140757	Str III	8,390 ± 50	7578 to 7337
Wadi Fidan 01 (73–75),			
Beta-1544599	Str III, first, B12077	8,200 ± 50	7449 to 7063
Beta-1544600	StrIII, first, B12187	8,000 ± 50	6760 to 6699
AA68192	Str IIA, AREA M, L44, B10461	7,973 ± 48	7047 to 6697
AA68193	Str IIB, AREA J, L237, B11545	8,104 ± 49	7319 to 6831
AA68194	Str IIB, AREA J, L244, B11733	8,142 ± 57	7341 to 6869
AA68195	Str IIB, AREA J, L259, B11887	8,007 ± 51	7064 to 6700
AA68196	Str IIB, AREA M, L14, B10093	8,107 ± 52	7321 to 6831
AA68197	Str IIB, AREA M, L17, B10092	8,205 ± 51	7450 to 7065
Wadi Fidan 61 (this study)			
AA102548	Str IV, L044, B30138 *Chenopodiaceae*	7,288 ± 52	6239 to 6030
AA102549	Str III, L054, B30185 *Pistacia atlantica*	7,517 ± 66	6467 to 6237
AA102550	Str IV L 076 B30282 *Tamarix sp.*	7,722 ± 54	6646 to 6460
AA102551	Str IV L 076 B30293 *Acacia sp.*	6,811 ± 51	5798 to 5623
AA102552	Str IV L 084 B30325 *Tamarix sp.*	7,671 ± 56	6638 to 6430
Wadi Fidan 51 (64)			
Beta-118580		6,260 ± 40	5316 to 5069

List of radiocarbon dates from literature and from this study, grouped per excavation site, the laboratory (Lab) codes for each sample, the context (Str., stratum; L, locus; B, basket) uncalibrated (uncal.) ^{14}C ages, calibrated using the OXCAL online tool [IntCal20 curve, by Reimer et al. (62)].

and susceptibility in units of $10^{-3}m^3$/kg), hereby referred as the FE ratio, is plotted in Fig. 2. Fig. 2*A* shows clusters of different materials from the four collections, with both the lowest and highest values of the FE ratio associated with the flints from Wadi Fidan 01 (orange squares). Ceramic fragments with handles from Wadi Fidan 61 (cyan Xs) display low NRM values, but higher susceptibilities, and have firing efficiencies of less than 100.

Fig. 2*B* shows only the specimens that passed our selection criteria (which do not include consideration of FE). All successful specimens have FE ratios between 100 and 1,000. With only one exception, the successful specimens had NRM values higher than 40 μAm^2/kg and a susceptibility higher than 2×10^{-4} m^3/kg. Successful flint specimens from Wadi Fidan 01 cluster between an NRM of 40 to 90 μAm^3/kg and a χ around 2×10^{-4} m^3/kg, while ceramic fragments from Wadi Fidan

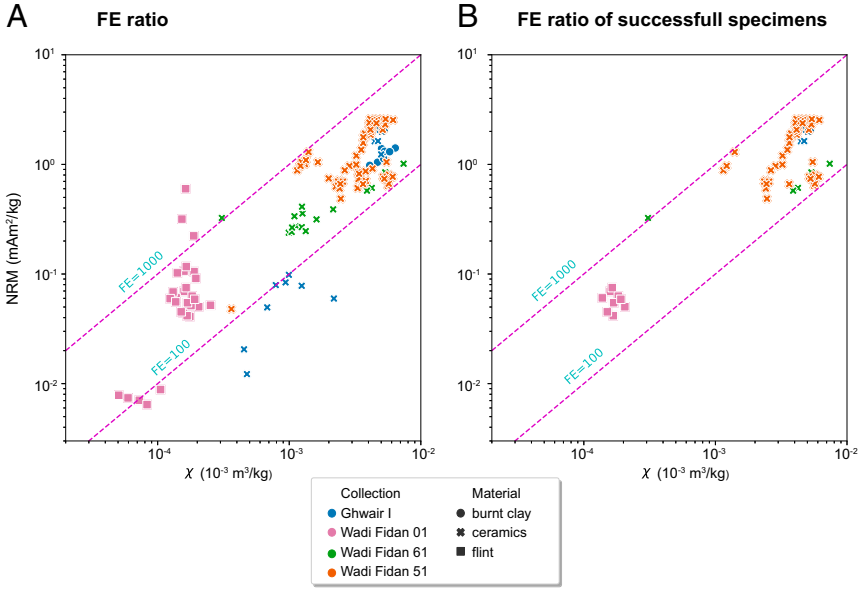

Fig. 2. FE ratio (FE plots) of the NRM (in $10^{-3}Am^2$/kg) vs. susceptibility χ (10^{-3} m^3/kg). The magenta dashed lines are FE ratios of 100 and 1,000. (*A*) All specimens analyzed in this study, sorted by archaeological excavation. (*B*) "Reliable" specimens, i.e., only those that passed our selection criteria for paleointensity.

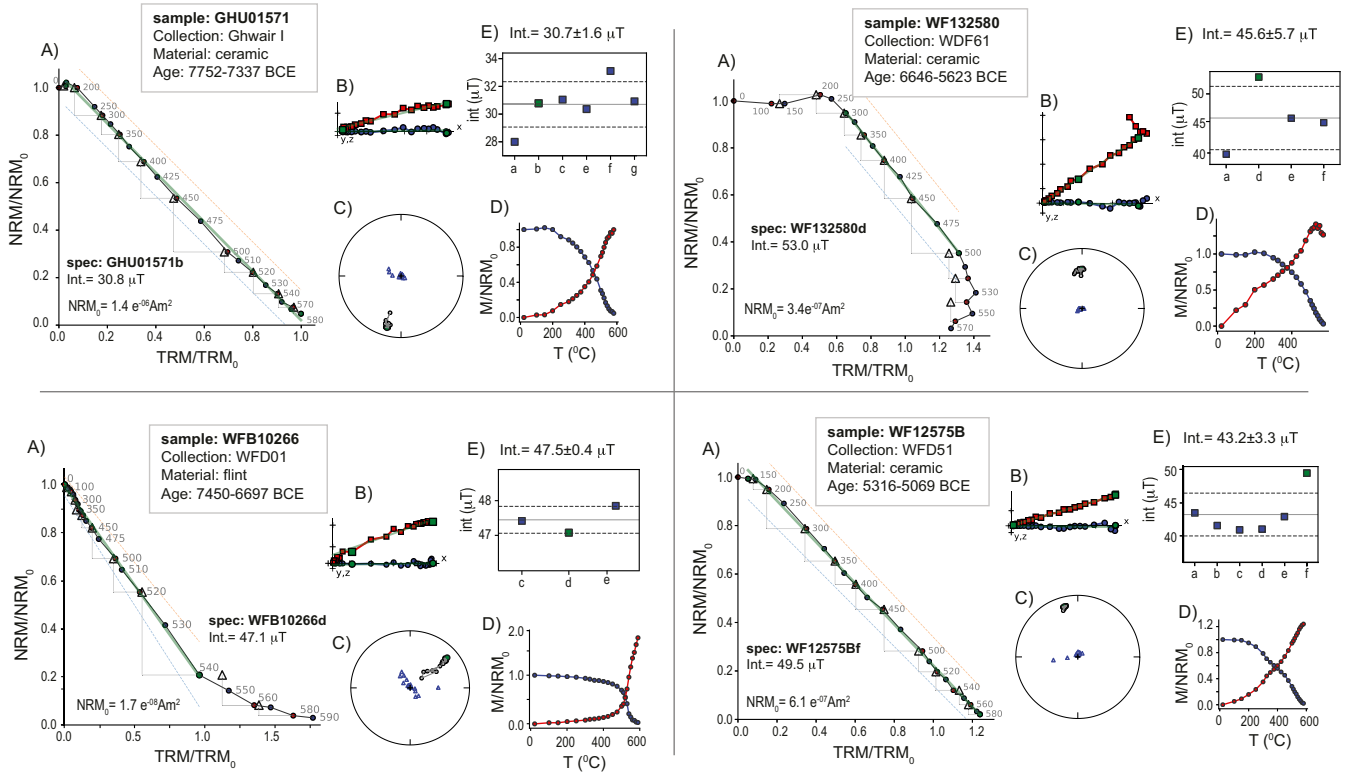

Fig. 3. Representative results from the paleointensity experiments from four specimens. Arai plots of representative specimens (*A*), Zijderveld diagrams (*B*), equal area projection (*C*), normalized magnetization (M/NRM_0) vs. temperature plot (*D*), and archaeointensity sample results (which here also corresponds to a paleointensity site, the smallest feature expected to have uniform age and magnetic properties) plot indicating all "successful" specimens and the average archaeointensity sample intensity (in μT) corrected for cooling rate and anisotropy of the thermal remanence (*E*). Results were processed and displayed using the Thellier_GUI.py program (51).

51 had a higher NRM, between 0.1 and 3 mAm^2/kg, and a χ between 1 and 8 $\times$ 10^{-4} m^3/kg). As there is no need to demagnetize specimens to measure the susceptibility, the NRM/χ ratio can be readily used as a preliminary test to select suitable specimens for future archaeointensity analyses. This is particularly useful for selecting flints, which may or may not have been fired prior to knapping. In the case of flints with FE ratios higher than 1,000, it is possible that they were remagnetized by lightning or exposure to magnetic fields during excavation.

Intensity. The results from the paleointensity experiments are summarized in Table 1 and Fig. 3. Overall, of the 129 initial specimens, 66 specimens passed the selection criteria, Cromwell's criteria (CCRIT) (47). The definitions of various statistics can be found in Paterson et al. (48). Here, the number of successful specimens per sample must be $\geq$3, with two or more partial thermal remanent magnetization (pTRM) checks, FRAC (the fraction of remanence used in the slope calculation, as defined by ref. 48) values of $\geq$0.78, scatter (=True), b–beta = 0.1, maximum angular deviation and deviation angle of 10, and $|\vec{k'}|$ [the curvature value of Paterson (49), as modified slightly by Cromwell et al. (47)] of <0.164. Typically, a successful specimen is characterized by a straight Arai plot (50) (e.g., Fig. 3, *Upper Left* and *Lower Right*). The sole exception to these rules is when the specimens are characterized by a clear two-component behavior in the directions (e.g., Fig. 3, *Upper Right*). Using these criteria, the success rate at specimen level is 51%. At the sample level, WF10095, WF102661, and WF102662 were rejected because only one or two specimens successfully recorded an intensity value (Fig. 4 and Table 1).

It is common in archaeointensity studies to use "box and whisker" plots. We prefer here to use the "violin" plot combined with a "swarm" plot of the individual data points (Fig. 4). The violin–swarm plot shows the distribution of data, and, unlike the box plot, no data are hidden. Box plots show quantiles of data in abrupt "boxes," while violin plots use a rotated kernel-density plot on each side. They are therefore similar to box plots, but also show the probability density of the data at different values, in this case, smoothed by a kernel-density estimator.

At the archaeological context level (where context refers to either the basket number representing the smallest level of artifact collection or locus/context, the feature or deposit where artifacts are located), one of the three contexts from Ghwair I, one of five from Wadi Fidan 01 (Tellet Ifdan), one of the two from Wadi Fidan 61, and eight of the nine contexts from Wadi Fidan 51 passed the strict selection criteria. The violin plot in Fig. 4 shows the distribution of all specimens by archaeological sample (individual fragment) that passed the selection criteria (white circles indicate the specimens with the relaxed FRAC criterion of FRAC $\geq$ 0.3 associated with two-component directional behavior). Five of the 14 samples are characterized by a symmetric SD around their median values, suggesting a normal distribution (GHU01571, WFB10266, WF12575D, WF12575E, and WF12575L), while four (WF132580, WF12575B, WF12575I, and WF12575M) show a higher dispersion in the intensity distribution with elongated tips. The latter four violins show an asymmetric bimodal distribution, where the lower values have a slightly higher frequency. In addition, two samples (WF10095 and WF102661) are represented by only two specimens and one (WF102662) by a single specimen; thus, they cannot be deemed as robust, and are discarded from further discussion.

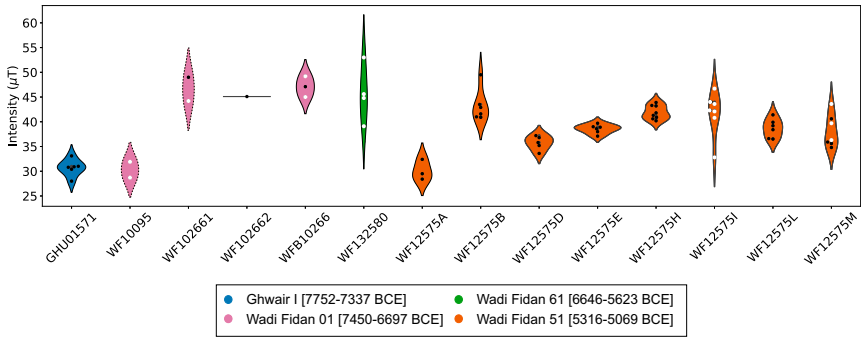

Fig. 4. Violin plot showing the intensity values from specimens that passed the selection criteria, grouped by archaeointensity sample, with kernel-density estimates of their statistical distribution. Black circles represent the specimens that passed the CCRIT criteria with a FRAC $\geq |0.78|$, and the white circles represent the specimens that passed the CCRIT criteria with a FRAC ≥ 0.3. Dashed contours represent the samples that did not pass the selection criteria at sample level.

After averaging by locus,* we obtained values of 30.8 ± 1.5 μT from Ghwair I locus 12.5 (averaged over 6 specimens; Table 1), 47.1 ± 2.1 μT from Wadi Fidan 01 (over 3 specimens from locus 37; Table 1), 47.2 ± 3.2 μT for Wadi Fidan 61 (averaged over 5 specimens from locus 2; Table 1), and, finally, an average value of 39.8 ± 2.7 μT for Wadi Fidan 51 (locus 601, averaged over 7 samples and 44 specimens, Table 1). The weighted errors for all loci are less than 6 μT.

Discussion

In this study, we obtained reliable paleointensity results from all four Pre-Pottery to Pottery Neolithic locations excavated in Jordan's Faynan district. The estimates range from the lowest value recorded from the Ghwair I (7752 to 7337 BCE) of 30.7 ± 1.6 μT to the highest values from Wadi Fidan 01 (7450 to 6697 BCE) and Wadi Fidan 61 (6646 to 5623 BCE) of 47.5 ± 0.4 μT and 45.6 ± 5.7 μT, respectively. Importantly, we obtained reliable results from all material analyzed, including flint. While pottery and several other clay-based materials are widely investigated in archaeomagnetic studies, the use of burnt chert is far less common (5–8), despite being the most common raw material for manufacturing of tools in the entire Paleolithic, Neolithic, and even the Bronze Age (4). Indeed, for at least 50 ky, stone tools have been produced by deliberately heating fine-grained siliceous rocks to improve their flaking properties, as heating helps to propagate fractures in the material, making it easier for production of the stone tools (10, 11, 52). Carrancho et al. (5) showed through experimental heating of flint (from a Miocene formation) that the acquired magnetization was characterized by a weak NRM carried by multidomain magnetite grains; hence, they failed in recording a reliable paleomagnetic signal. In contrasting examples, Kapper et al. (6) and Zeigen et al. (8) successfully extracted paleointensity data from Neolithic flint from Italy and Paleolithic flint from Israel, respectively. The discrepancy among these studies can be explained by the fact that flint can show varying degrees of enhancement of magnetic properties upon heating to temperatures above 400 to 500°C, linked to magnetite formation (5, 9, 53, 54).

We calculated the VADM (in ZAm^2) to compare the paleointensities obtained in this study to the global models (35) and available in the literature for a similar age range (Fig. 1). We obtained a value of 59.5 ± 3.1 ZAm^2 for Ghwair locus 12.5, values of 92.0 ± 0.7 ZAm^2 for Wadi Fidan 01, 88.4 ± 11.1 ZAm^2 for Wadi Fidan 61, and, finally, values ranging from 58.3 ± 4.1 to 83.7 ± 6.3 ZAm^2 for Wadi Fidan 51 (Table 1).

Our data can be compared with the PSV curves calculated for Jordan from the available global models: the CALS10k.2 and HFM.OL1.A1 global models [blue and orange curves in Fig. 1 (35, 36)], SHA.DIF.14K [black line in Fig. 1 (36)], and SHAWQIA/SHAWQ2k models [red line in Fig. 1 (26, 37)]. From older to younger ages, the value from Ghwair I (7752 to 7337 BCE) of 59.7 ZAm^2 is lower than expected values from the PSV curve calculated from the global models (Fig. 1), while the values from Wadi Fidan 01, 61, and 51 are in agreement with the paleointensity values predicted by the global models, ranging between 90 and 70 ZAm^2 from ∼7000 to ∼5200 BCE. Indeed, the models show an important increase in the geomagnetic field strength of 40 ZAm^2 (from ∼60 ZAm^2 to ∼100 ZAm^2) from 8000 y until 7000 BCE, thus in a relatively short amount of time of ∼600 y. This rate of change would correspond about 4 ZAm^2 per c., although additional data are needed to understand such geomagnetic field behavior. After about 6000 BCE, the VADMs decrease to ∼50 ZAm^2 and remain constant until ∼2500 BCE.

When compared with the available archaeomagnetic studies from an area of about 600 km^2, the data from Wadi Fidan 01, 61, and 51 compare remarkably well with the data from Northern Iraq (55) and Syria between 6800 and 5000 BCE (40). Prior to this study, Gallet et al. (40) in northern Mesopotamian provided the oldest Middle Eastern paleointensity data in the GEOMAGIA50 database, recovered from two Late Neolithic sites (Tell Halula and Tell Masaïkh) in Syria, with ages ranging from ∼7000 BC and ∼5000 BC. Our results from Ghwair I and Wadi Fidan 01 now represent the oldest archaeointensity data from outside Japan (56) and Siberia (57, 58), to which they cannot be compared due to the geographical distance.

The data presented here provide the oldest and (one of the) lowest archaeointensity values of the Levant, ancient Mesopotamia, Turkey, and Europe, and, together with Gallet et al. (40), provide a unique opportunity to investigate changes of the geomagnetic field strength from ∼7750 to ∼5000 BCE. In particular, they reveal rates of changes from ∼7750 to 7000 of 4 ZAm^2/c., a value remarkably similar to the 500-y period preceding the occurrence of the LIAA, between 1800 and 1200 BCE. While much faster rates of change in the secular variations are found during the LIAA, with 61 ZAm^2/c. (25), the value recorded in Jordan is higher than the 5 ky preceding the LIAA, with rates of 0.5 ZAm^2/c. or lower. Therefore,

*Please note that the archaeological site does not correspond to the paleointensity site. We consider the archaeological site as the excavation, e.g., Ghwair. We consider paleeointensity site as the smallest group of samples that we expect to yield the same archaeomagnetic signal, i.e., same firing instant, which can be averaged out. In this study, we consider each sample, ceramic or flint fragment, as an individual site because it is not possible to independently determine if different fragments were produced or last fired at the same historical moment.

moderately rapid changes are suggested to have occurred during the Holocene and remain undetected due to the low resolution of archaeointensity data during the Holocene and Pleistocene.

Finally, improving the spatial and temporal distribution of archaeomagnetic data both helps refining the resolution of the use of the database as a dating tool and helps in understanding the behavior of the EMF of the Holocene by enhancing the resolution and robustness of the geomagnetic models.

Conclusions

Here, we present high-quality archaeointensity data from Jordan spanning from 7752 to 5069 BCE, thus the oldest record from the Levant, Turkey, Egypt, and ancient Mesopotamia.

- We investigated 129 archaeological specimens of pottery, burnt clay, and burnt flint selected from four Neolithic archaeological sites (Ghwair I and Wadi Fidan 01, 61, and 51).
- The high-quality paleointensity results were obtained with the IZZI protocol and applying a strict selection criteria.
- The paleointensity results from Jordan vary from values of 30.7 $\pm$ 1.6 μT (or 59.5 $\pm$ 3.1 ZAm^2) from the Ghwair I excavation site, values of 47.5 $\pm$ 0.4 μT (92.0 $\pm$ 0.7 ZAm^2) for Wadi Fidan 01, 45.6 $\pm$ 5.7 μT (or 88.4 $\pm$ 11.1 ZAm^2) for Wadi Fidan 61, and, finally, values ranging from 30.1 $\pm$ 2.1 to 43.2 $\pm$ 3.3 (or 58.3 $\pm$ 4.1 to 83.7 $\pm$ 6.3 ZAm^2) for Wadi Fidan 51 (Table 1).
- These results suggest that one of the weakest field values of the last 10 ky in the Levant occurred around 7600 BCE, recovering its strength at a relatively rapid rate until around 7000 and weakening gradually until 5200 BCE. These values compare well to the values predicted by the global geomagnetic models and the data from Northern Iraq (59) and Syria (40).
- By successfully investigating the archaeointensity of flint, we demonstrate the potential and applicability of the use of this material, which is the most common raw material for the manufacturing of tools throughout most of human history, and yet rarely investigated.
- Finally, these results will help enhance paleomagnetic global and regional field models and improve the use of archaeomagnetism as an independent and robust dating tool.

Materials and Methods

Archaeological Context. The Neolithic period in the southern Levant is long, spanning the Pre-Pottery Neolithic and Pottery Neolithic periods and spanning ~10,200 to 7,500 y B.P. The samples analyzed in this study (Fig. 5 and Table 1) were selected from Neolithic excavations in the Faynan copper ore region of southern Jordan and include: Ghwair I, a Middle PPNB settlement, from ca. 9,710 to 8,390 y B.P. (60); Wadi Fidan 01 spanning the Pre-Pottery Neolithic period from ca. 8,270 to 7,970 y B.P.; Wadi Fidan 61, ca. 7,670 to 6,880 y B.P.; and Wadi Fidan 51 dating to the Pottery Neolithic to Neolithic, ca. 8,250 to 7,800 y B.P. (38, 43, 61). The radiocarbon dates were obtained from charcoal samples and were calibrated here by using the OxCal online tool [IntCal20 curve, by Reimer et al. (62); Table 2]. Regarding age determination, it is important to note the differences between a typical paleomagnetic sampling "site" (e.g., a basalt outcrop of a particular lava flow) and an archaeological site used in archaeomagnetic research. While the former represents, per definition, a specific incident in time that can be determined by the pooled mean age of all chronometric results from the site, the latter typically represents a wide time range, which corresponds to the entire occupation span of the specific location. In fact, even in the narrower levels of the archaeological "layer" and "locus," the heating events of individual pottery sherds and flint items might correspond to different firing ages. Accordingly, it is often most appropriate to provide the entire range of calibrated dates for a given context, and when statistical treatments are done, they should be based on specific, known variables (e.g., context type, relative stratigraphy, etc.). In the present case, each of the investigated archaeological sites represents long, continuous occupation spans (up to several hundred years), which is often the case for similar sites from the Neolithic period (42). Accordingly, we provide the entire age ranges associated with the strata from which we took individual samples.

The Ghwair I and Wadi Fidan 01 are especially important for the Neolithic period in southern Jordan because they span the Middle Pre-Pottery Neolithic Period and the end of the Late Pre-Pottery Neolithic period (WFD 01 to Tel Tifdan). Our age estimates were made by first acquiring the radiocarbon dates (Table 2) and then placing the dates into the accepted scholarly chronological framework established for the southern Levant Pre-Pottery Neolithic period (38) and the Pottery Neolithic Period (41).

The Ghwair I settlement (60) (Fig. 1), situated along the Wadi Ghwair that drains into the main Wadi Faynan, was excavated by Najjar and Simmons (60) and dated to the Middle PPNB (calibrated age of 9700 to 8390 or 7983 to 7571 BCE). These excavations revealed four main undisturbed occupation strata and spectacularly preserved architectural features, including intact walls standing over 2 m high (63). From this excavation site,

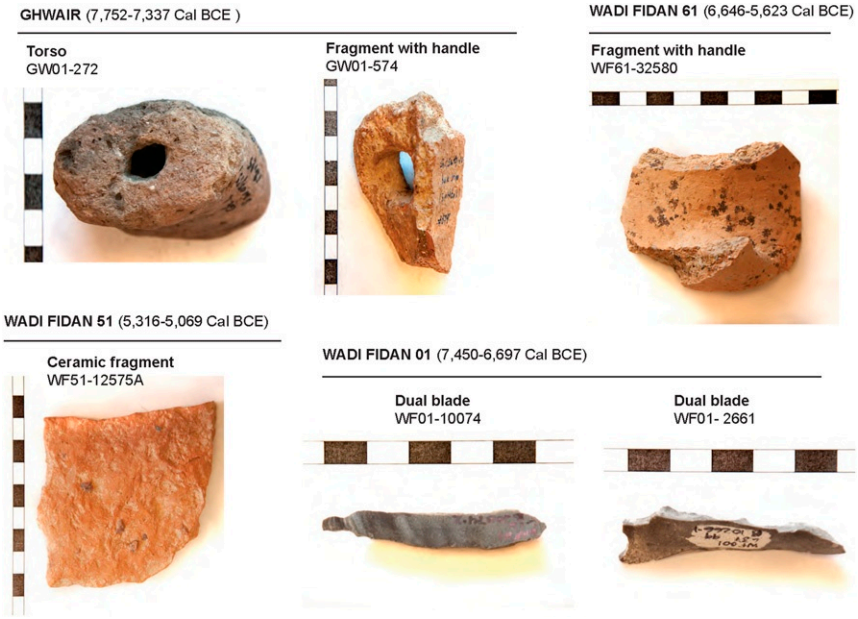

Fig. 5. Details of some of the archaeological materials analyzed in this study, reported per archaeological excavation, calibrated radiocarbon age, and description.

we analyzed a fragment of a statuette torso and two fragments of pottery (Fig. 5 and Table 1), all belonging to the third occupation stratum, with an age of 7752 to 7337 BCE (2σ, from four radiocarbon dates; Table 2).

The Wadi Fidan 01 (Tellet Ifdan) excavations were carried out by Levy, Najjar, and Adams in 1999 where three main occupation strata were defined and dated 7450 to 6697 BCE (calibrated from eight radiocarbon dates from three strata; Table 2). From these excavations, we analyzed five burnt crested blades made of flint from two strata where intense burning took place at the site (Fig. 5 and Table 1).

The Edom Lowlands Regional Archaeology Project (ELRAP) Wadi Fidan 61 excavations were carried out by Levy and Najjar in 2013. The excavation site is dated 6646 to 5623 BCE (2σ, calibrated from five ^{14}C; Table 2). We analyzed two pottery fragments from two different loci (Fig. 5 and Table 1). To date, this is the largest Pottery Neolithic site identified in the Faynan region and is situated $\sim$20 km west of the Wadi Fidan gorge.

Small-scale excavations were carried out at the Wadi Fidan 51 excavation site by the ELRAP team and dated to the transition of the Pottery Neolithic to early Chalcolithic at 5316 to 5069 BCE (2σ; uncalibrated radiocarbon was 6260 $\pm$ 40 y B.P. (64), and Table 2. We analyzed nine pottery fragments from one locus (Fig. 5 and Table 1).

Analyses.

FE ratio analyses. A total of 129 specimens were prepared for paleointensity experiments, selecting six to eight fragments per archaeological object (sample). All specimens were measured for the NRM and susceptibility (χ), a nondimensional parameter controlled by the volume concentration of ferromagnetic minerals. NRM and χ can be plotted against each other and compared to various slopes (Königsberger or *Q* ratio), usually adopted as a measure of the rock's magnetic efficiency. As the Königsberger ratio was intended to assess the likely source of local magnetic anomalies by comparing the remanent to the induced field, it is not as useful for this purpose, which is to assess the efficiency of magnetization. In particular, we wish to ascertain whether a particular artifact was fired, which would result in a higher efficiency than unfired materials. Therefore, we use the ratio of the mass normalized NRM to χ, similarly to Schnepp (65), here called FE, and not K_q. In this study, low FEs result from low efficiency of magnetization, presumably because the sample was never fired to high temperature. Higher values of FE result from a thermal origin of the NRM, and we interpret those samples with FE ratios higher than about 100 (magenta dashed lines in Fig. 2) as being thermal remanent magnetizations (TRMs). One caveat to this assumption is for the case in which specimens were exposed to magnetic fields (e.g., by being struck by lightning or exposed to magnets during excavation). In that case, the NRM would be an isothermal remanent magnetization, and not a TRM.

Paleointensity analyses. All specimens were analyzed by using the paleointensity IZZI protocol of Yu et al. (45) and Tauxe and Staudigel (46). The IZZI method combines two variations of the Thellier–Thellier (1) method, the IZ protocol of Aitken et al. (66), and the ZI protocol of Coe (67) and includes the pTRM checks of Coe et al. (68). The IZZI approach therefore incorporates a check for alteration during the experiments and a test meant to detect the failure of the so-called "Reciprocity Law" of ref. 1. Here, we performed 50 heating steps per experiment in four experiments at two different laboratory fields (30 and 60 μT). Data as shown in Table 1 were subsequently corrected for the cooling rate [CR; correcting for the difference between the duration of the laboratory experiments and archaeological cooling (69)] and for the anisotropy [ATRM; a correction for a preferred alignment of the ferromagnetic distort the magnetization record (70–72)]. Both CR and ATRM corrections did not change the final values; indeed, the CR correction varied from a factor of 0.88 to 1.01 (0.96 on average) and ATRM correction of a factor from 0.85 to 1.22 (0.99 on average).

Data Availability. Rock and paleomagnetic data have been deposited in the Magnetics Information Consortium database (https://earthref.org/MagIC/17126).

ACKNOWLEDGMENTS. This work was supported in part by US–Israel Binational Science Foundation Grant 2018305 (to L.T. and E.B.-Y.), a NEXTData grant (to F.F. and A.D.C.), and NSF Grant EAR1547263 (to L.T.). We thank Shuhui Cai for discussions regarding FE. We thank Ghazi Bisheh, former Director General of the Department of Antiquities of Jordan, for making the fieldwork possible. Funding for fieldwork at Wadi Fidan 01 and 51 was provided by the C. Paul Johnson Family Foundation; fieldwork at Wadi Fidan 61 provided by Reuben and Norma Kershaw Family Foundation and Jerome and Miriam Katzin Family Foundation; Ghwair I field work was supported by the NSF (Grant SBR-9708241), the National Geographic Society (Grant 6033-97), the Brennan Foundation, and the University of Nevada at Las Vegas (to A. Simmons).

1. E. Thellier, O. Thellier, Sur l'intensité du champ magnétique terrestre dans le passé historique et géologique. *Ann. Geophys.* **15**, 285–378 (1959).
2. M. J. Aitken, Dating by archaeomagnetic and thermoluminescent methods. *Philos. Trans. R. Soc. Lond. A* **269**, 77–88 (1970).
3. R. Thér *et al*., How was Neolithic pottery fired? An exploration of the effects of firing dynamics on ceramic products. *J. Archaeol. Method Theory* **26**, 1143–1175 (2019).
4. A. N. Goring-Morris, E. Hovers, A. Belfer-Cohen, *The Dynamics of Pleistocene and Early Holocene Settlement Patterns and Human Adaptations in the Levant: An Overview* (Oxbow Books, Oxford, UK, 2009).
5. A. Carrancho, J. Morales, A. Goguitchaichvili, R. Alonso, M. Terradillos, Thermomagnetic monitoring of lithic clasts burned under controlled temperature and field conditions. Implications for archaeomagnetism. *Geofis. Int.* **53**, 473–490 (2014).
6. K. Kapper, F. Donadini, A. M. Hirt, Holocene archeointensities from mid European ceramics, slags, burned sediments and cherts. *Phys. Earth Planet. Inter.* **241**, 21–36 (2015).
7. K. Kapper, F. Donadini, M. Mauvilly, S. Panovska, A. M. Hirt, New directional archeomagnetic data of burned cave sediments from Switzerland and geomagnetic field variations in Central Europe. *Geophys. J. Int.* **198**, 1208–1221 (2014).
8. C. Zeigen, R. Shaar, Y. Ebert, E. Hovers, Archaeomagnetism of burnt cherts and hearths from Middle Palaeolithic Amud Cave, Israel: Tools for reconstructing site formations processes and occupation history. *J. Archaeol. Sci.* **107**, 71–86 (2019).
9. G. J. Borradaile, S. A. Kissin, J. D. Stewart, W. A. Ross, T. Werner, Magnetic and optical methods for detecting the heat treatment of chert. *J. Archaeol. Sci.* **20**, 57–66 (1993).
10. B. A. Purdy, H. K. Brooks, Thermal alteration of silica minerals: An archeological approach. *Science* **173**, 322–325 (1971).
11. S. Weiner, V. Brumfeld, O. Marder, O. Barzilai, Heating of flint debitage from Upper Palaeolithic contexts at Manot Cave, Israel: Changes in atomic organization due to heating using infrared spectroscopy. *J. Archaeol. Sci.* **54**, 45–53 (2015).
12. D. Atkinson, J. A. King, "Fine particle magnetic mineralogy of archaeological ceramics" in J. Physics: Conference Series (IOP Publishing, Bristol, UK, 2005), vol. **17**, p. 145.
13. A. Genevey, Y. Gallet, J.-C. Margueron, Eight thousand years of geomagnetic field intensity variations in the eastern Mediterranean. *J. Geophys. Res. Solid Earth* **108**, 2228 (2003).
14. E. Ben-Yosef *et al*., Application of copper slag in geomagnetic archaeointensity research. *J. Geophys. Res.* **113**, B08101 (2008).
15. E. Ben-Yosef *et al*., Geomagnetic intensity spike recorded in high resolution slag deposit in Southern Jordan. *Earth Planet. Sci. Lett.* **287**, 529–539 (2009).
16. R. Shaar *et al*., Geomagnetic field intensity: How high can it get? How fast can it change? Constraints from Iron Age copper slag. *Earth Planet. Sci. Lett.* **301**, 297–306 (2011).
17. E. Ben-Yosef, M. Millman, R. Shaar, L. Tauxe, O. Lipschits, Six centuries of geomagnetic intensity variations recorded by royal Judean stamped jar handles. *Proc. Natl. Acad. Sci. U.S.A.* **114**, 2160–2165 (2017).
18. R. Shaar *et al*., Large geomagnetic field anomalies revealed in Bronze to Iron Age archeomagnetic data from Tel Megiddo and Tel Hazor, Israel. *Earth Planet. Sci. Lett.* **442**, 173–185 (2016).
19. S. Cai *et al*., Geomagnetic intensity variations for the past 8 kyr: New archaeointensity results from Eastern China. *Earth Planet. Sci. Lett.* **392**, 217–229 (2014).
20. R. Shaar, L. Tauxe, A. Goguitchaichvili, M. Devidze, V. Licheli, Further evidence of the Levantine Iron Age geomagnetic anomaly from Georgian pottery. *Geophys. Res. Lett.* **44**, 2229–2236 (2017).
21. P. W. Livermore, A. Fournier, Y. Gallet, Core-flow constraints on extreme archeomagnetic intensity changes. *Earth Planet. Sci. Lett.* **387**, 145–156 (2014).
22. Y. Gallet, A. Genevey, M. Le Goff, F. Fluteau, S. A. Eshraghi, Possible impact of the Earth's magnetic field on the history of ancient civilizations. *Earth Planet. Sci. Lett.* **246**, 17–26 (2006).
23. P. Ertepinar *et al*., Extreme geomagnetic field variability indicated by Eastern Mediterranean full-vector archaeomagnetic records. *Earth Planet. Sci. Lett.* **531**, 115979 (2020).
24. S. Cai *et al*., Archaeointensity results spanning the past 6 kiloyears from eastern China and implications for extreme behaviors of the geomagnetic field. *Proc. Natl. Acad. Sci. U.S.A.* **114**, 39–44 (2017).
25. M. Korte, C. G. Constable, Archeomagnetic intensity spikes: Global or regional geomagnetic field features? *Front. Earth Sci.* **6**, 1–15 (2018).
26. M. L. Osete *et al*., Two archaeomagnetic intensity maxima and rapid directional variation rates during the Early Iron Age observed at Iberian coordinates. Implications on the evolution of the Levantine Iron Age Anomaly. *Earth Planet. Sci. Lett.* **533**, 116047 (2020).
27. G. M. Turner, R. Kinger, B. McFadgen, M. Gevers, The first archaeointensity records from New Zealand: Evidence for a fifteenth century AD archaeomagnetic 'spike' in the SW Pacific Region? *Geol. Soc. Lond. Spec. Publ.* **497**, 47–72 (2020).
28. I. Peters, L. Tauxe, E. Ben-Yosef, Archaeomagnetic dating of pyrotechnological contexts: A case study for copper smelting sites in the Central Timna Valley, Israel. *Archaeometry* **60**, 544–570 (2018).
29. M. Gómez-Paccard *et al*., Archaeomagnetic and rock magnetic study of six kilns from North Africa (Tunisia and Morocco). *Geophys. J. Int.* **189**, 169–186 (2012).

30. M. D. Stillinger, J. W. Hardin, J. M. Feinberg, J. A. Blakely, Archaeomagnetism as a complementary dating technique to address the Iron Age chronology debate in the Levant. *Near East. Archaeol.* **79**, 90–106, 2016.
31. E. Ben Yosef, L. Tauxe, T. E. Levy, Archaeomagnetic dating of copper smelting site F2 in the Timna Valley (Israel) and its implications for the modelling of ancient technological developments. *Archaeometry* **52**, 110–1121 (2010).
32. D. Hnatyshin, V. A. Kravchinsky, Paleomagnetic dating: Methods, MATLAB software, example. *Tectonophysics* **630**, 103–112 (2014).
33. F. J. Pavón-Carrasco, J. Rodríguez-González, M. L. Osete, J. M. Torta, A Matlab tool for archaeomagnetic dating. *J. Archaeol. Sci.* **38**, 408–419 (2011).
34. M. C. Brown *et al*., GEOMAGIA50. v3: 1. General structure and modifications to the archeological and volcanic database. *Earth Planets Space* **67**, 83 (2015).
35. C. Constable, M. Korte, S. Panovska, Persistent high paleosecular variation activity in Southern Hemisphere for at least 10 000 years. *Earth Planet. Sci. Lett.* **453**, 78–86 (2016).
36. F. J. Pavón-Carrasco, M. L. Osete, J. M. Torta, A. De Santis, A geomagnetic field model for the Holocene based on archaeomagnetic and lava flow data. *Earth Planet. Sci. Lett.* **388**, 98–109 (2014).
37. S. A. Campuzano, M. Gómez-Paccard, F. J. Pavón-Carrasco, M. L. Osete, Emergence and evolution of the South Atlantic Anomaly revealed by the new paleomagnetic reconstruction SHAWQ2k. *Earth Planet. Sci. Lett.* **512**, 17–26 (2019).
38. I. Kuijt, A. N. Goring-Morris, Foraging, farming, and social complexity in the Pre-Pottery Neolithic of the Southern Levant: A review and synthesis. *J. World Prehist.* **16**, 361–440 (2002).
39. B. Finlayson *et al*., Architecture, sedentism, and social complexity at Pre-Pottery Neolithic A WF16, Southern Jordan. *Proc. Natl. Acad. Sci. U.S.A.* **108**, 8183–8188 (2011).
40. Y. Gallet *et al*., New Late Neolithic (c. 7000–5000 BC) archeointensity data from Syria. reconstructing 9000 years of archeomagnetic field intensity variations in the Middle East. *Phys. Earth Planet. Inter.* **238**, 89–103 (2015).
41. E. B. Banning, "It's a Small World: Work, Family Life, and Community in the Late Neolithic" in *The Social Archaeology of the Levant: From Prehistory to the Present*, A. Yasur-Landau, E. H. Cline, Y. Rowan, Eds. (Cambridge University Press, Cambridge, UK, 2018), pp. 98–121.
42. O. Gary, "Rollefson. The Neolithic Period" in *Jordan: An Archaeological Reader*, R. B. Adams, Ed. (Equinox, London, UK, 2008), pp. 71–108.
43. O. Bar-Yosef, "The "Pre-Pottery Neolithic" period in the Southern Levant" in *Préhistoire du Levant*, J. Chauvin, P. Sanlaville, Eds. (CNRS, Paris, France, 1981), pp. 551–570.
44. K. V. Flannery, The origins of the village revisited: From nuclear to extended households. *Am. Antiq.* **67**, 417–433 (2002).
45. Y. Yu, L. Tauxe, A. Genevey, Toward an optimal geomagnetic field intensity determination technique. *Geochem. Geophys. Geosyst.* **5**, Q02H07 (2004).
46. L. Tauxe, H. Staudigel, Strength of the geomagnetic field in the Cretaceous Normal Superchron: New data from submarine basaltic glass of the Troodos Ophiolite. *Geochem. Geophys. Geosyst.* **5**, Q02H06 (2004).
47. G. Cromwell, L. Tauxe, H. Staudigel, H. Ron, Paleointensity estimates from historic and modern Hawaiian lava flows using basaltic volcanic glass as a primary source material. *Phys. Earth Planet. Inter.* **241**, 44–56 (2015).
48. G. A. Paterson, L. Tauxe, A. J. Biggin, R. Shaar, L. C. Jonestrask, On improving the selection of Thellier-type paleointensity data. *Geochem. Geophys. Geosyst.* **15**, 1180–1192 (2014).
49. G. A. Paterson, A simple test for the presence of multidomain behavior during paleointensity experiments. *J. Geophys. Res.* **116**, B10104 (2011).
50. T. Nagata, Y. Arai, K. Momose, Secular variation of the geomagnetic total force during the last 5000 years. *J. Geophys. Res.* **68**, 5277–5282 (1963).
51. R. Shaar, L. Tauxe, Thellier GUI: An integrated tool for analyzing paleointensity data from Thellier-type experiments. *Geochem. Geophys. Geosyst.* **14**, 677–692 (2013).
52. M. Domanski, J. A. Webb, Effect of heat treatment on siliceous rocks used in prehistoric lithic technology. *J. Archaeol. Sci.* **19**, 601–614 (1992).
53. J. C. Larrasoaña *et al*., Magnetic properties of cherts from the Basque-Cantabrian Basin and surrounding regions: Archeological implications. *Front. Earth Sci.*, 10.3389/feart.2016.00035 (2016).
54. M. Moník, Z. Nerudová, P. Schnabl, Experimental heating of Moravian cherts and its implication for paleolithic chipped stone assemblages. *Archaemetry* **59**, 1190–1206 (2017).
55. I. E. Nachasova, K. S. Burakov, Geomagnetic variations in the VI-V millennia BC. *Geomagn. Aeron.* **38**, 502–505 (1998).
56. K. Kitazawa, Intensity of the geomagnetic field in Japan for the past 10,000 years. *J. Geophys. Res.* **75**, 7403–7411 (1970).
57. K. S. Burakov, I. E. Nachasova, G. N. Petrova, The geomagnetic field intensity in the Baikal region during the last millennia. *Geomagn. Aeron.* **40**, 219–223 (2000).
58. I. E. Nachasova, K. S. Burakov, O. V. Pilipenko, Variations in the intensity of the geomagnetic field in Siberia during the last 13000 years. *Izvestiya Physics of the Solid Earth* **51**, 44–50 (2015).
59. I. E. Nachasova, K. S. Burakov, Archaeointensity of the geomagnetic field in the fifth millennium BC in northern Mesopotamia. *Geomagn. Aeron.* **35**, 398–402 (1995).
60. A. H. Simmons, M. Najjar, Ghwair I: A small, complex Neolithic community in Southern Jordan. *J. Field Archaeol.* **31**, 77–95 (2006).
61. G. O. Rollefson, The aceramic Neolithic. *Bar Int. Ser.* **705**, 102–126 (1998).
62. P. J. Reimer *et al*., The IntCal20 Northern Hemisphere radiocarbon age calibration curve (0–55 cal kBP). *Radiocarbon* **62**, 725–757 (2020).
63. H.A. Simmons, *The Neolithic Revolution in the Near East: Transforming the Human Landscape* (University of Arizona Press, Tucson, AZ, 2011).
64. M. Burton, T. E. Levy, The Chalcolithic radiocarbon record and its use in southern Levantine archaeology. *Radiocarbon* **43**, 1223–1246 (2001).
65. E. Schnepp, Geomagnetic paleointensities derived from volcanic rocks of the Quaternary East Eifel volcanic field, Germany. *Phys. Earth Planet. Inter.* **94**, 23–41 (1996).
66. M. J. Aitken, A. L. Allsop, G. D. Bussell, M. B. Winter, Determination of the intensity of the Earth's magnetic field during archeological times: Reliability of the Thellier technique. *Rev. Geophys.* **26**, 3–12 (1988).
67. R. S. Coe, The determination of paleo-intensities of the Earth's magnetic field with emphasis on mechanisms which could cause non-ideal behavior in Thellier's method. *J. Geomag. Geoelectr.* **19**, 157–178 (1967).
68. R. S. Coe, S. Grommé, E. A. Mankinen, Geomagnetic paleointensities from radiocarbon-dated lava flows on Hawaii and the question of the Pacific nondipole low. *J. Geophys. Res.* **83**, 1740–1756 (1978).
69. M. J. Aitken, P. A. Alcock, G. D. Bussell, C. J. Shaw, Archaeomagnetic determination of the past geomagnetic intensity using ancient ceramics: Allowance for anisotropy. *Archaeometry* **23**, 53–64 (1981).
70. J. Rogers, J. M. W. Fox, M. J. Aitken, Magnetic anisotropy in ancient pottery. *Nature* **277**, 644–646 (1979).
71. R. J. Veitch, An investigation of the intensity of the geomagnetic field during Roman times using magnetically anisotropic bricks and tiles. *Arch. Sci. Geneve.* **37**, 359–373 (1984).
72. A. R. Biedermann, D. Bilardello, M. Jackson, L. Tauxe, J. M. Feinberg, Grain-size-dependent remanence anisotropy and its implications for paleodirections and paleointensities—Proposing a new approach to anisotropy corrections. *Earth Planet. Sci. Lett.* **512**, 111–123 (2019).
73. T. E. Levy *et al*., Early metallurgy, interaction, and social change: The Jabal Hamrat Fidan (Jordan) research design and 1998 archaeological survey. Preliminary report. *Hawliyyat Dairat al-Atar al-Ammat* **45**, 159–187 (2001).
74. A. Hauptmann, *The Archaeometallurgy of Copper: Evidence from Faynan, Jordan* (Springer Science & Business Media, Berlin, Germany, 2007).
75. M. M. Burton *et al*., Ceramic technology at Wadi Fidan 61, an early Pottery Neolithic site (ca. 6500 B.C.E.) in the Faynan region of southern Jordan. *J. Archaeol. Sci. Rep.* **38**, 103029 (2021).